To order $(\ln t)^{-1}$, the first term in the above expression and the first term in Eq. (B3) cancel leaving

$$\mathrm{Re}\Sigma_{11}(\vec{p}, p^0) = \frac{-8\pi n_0}{\ln[p^0 a^2 + 2\mu a^2 - (pa/2)^2]} .$$

Restricting ourselves further to the regime

$$pa \ll p_c a = (-16\pi n a^2/\ln n a^2)^{1/2} = 2(\mu a^2)^{1/2} ,$$

we find that the third term in the argument of the logarithm can be ignored with respect to the second.

The important values of $p^0$ are those near the poles of the Green's function where $p^0$ has the magnitude

$$p^0 = \omega_p \approx \tfrac{1}{2} p_c p \quad \text{for } p \ll p_c .$$

Therefore, the ratio of the first to the second term in the argument of the logarithm is

$$p^0/2\mu \approx p_c p/4\mu = p/p_c \ll 1 .$$

From Eq. (B2) for $s$, it can now be seen that $s$ is approximately equal to $2\mu a^2$ which, from Eq. (13) of the text, is small compared to unity. Therefore the most important part of the integral in Eq. (B1) does come from $qa$ much less than unity as assumed.

We have found that

$$\mathrm{Re}\Sigma_{11}(\vec{p}, p^0) = -8\pi n_0/\ln 2\mu a^2 = -8\pi n/\ln n a^2 + O[1/(\ln n a^2)^2] = 2\mu + O[1/(\ln n a^2)^2] ,$$

in the region $p \ll p_c$, $p^0 \approx \omega_p$.

*Research supported by the National Science Foundation.

[1]W. D. McCormick, D. L. Goodstein, and J. G. Dash, Phys. Rev. 168, 249 (1968); G. A. Stewart and J. G. Dash, Phys. Rev. A 2, 918 (1970).

[2]See, for example, J. G. Dash, Phys. Rev. A 1, 7 (1970) and references therein; H. W. Jackson, Phys. Rev. 180, 184 (1969); A. D. Novacov and F. J. Milford, J. Low Temp. Phys. (to be published); M. Schick and C. E. Campbell, Phys. Rev. A 2, 1591 (1970).

[3]P. C. Hohenberg, Phys. Rev. 158, 383 (1967).

[4]G. A. Stewart and J. G. Dash, see Ref. 1.

[5]S. T. Beliaev, Zh. Eksperim. i Teor. Fiz. 34, 433 (1958) [Soviet Phys. JETP 7, 299 (1957)].

[6]N. M. Hugenholtz and D. Pines, Phys. Rev. 116, 489 (1959).

PHYSICAL REVIEW A VOLUME 3, NUMBER 3 MARCH 1971

# High-Energy Neutron Scattering Measurements on Liquid Helium and Bose Condensation in He II †

O. K. Harling

*Battelle Memorial Institute, Pacific Northwest Laboratory, Richland, Washington* 99352

(Received 27 July 1970)

Differential neutron scattering cross sections for liquid $^4$He have been obtained for momentum transfers along the free-particle excitation curve up to 20.3 Å$^{-1}$. Momentum transfers in this range are much higher than in previously reported work. The measured recoil energies as well as the angular dependence of the scattering confirm that the neutron scattering, at these high values of $\kappa$, is sensitive to the motions of single helium atoms. A temperature dependence in the widths of the cross-section peaks, as well as shape changes in these peaks as the temperature is decreased below $T_\lambda$, is consistent with the idea that a narrow condensate component contributes to the scattering for $T < T_\lambda$. Results from a detailed comparison of the measured cross sections with a theory for high-energy neutron scattering are reported. The kinetic energy per liquid-helium atom is deduced from this theory-experiment comparison and is found to be in agreement with computations of the kinetic energy based on thermodynamic phase equilibria considerations. A fractional occupation of the zero-momentum condensate state of $(8.8 \pm 1.3)\%$ at 1.27 °K is also deduced from this theory-experiment comparison.

## I. INTRODUCTION

At sufficiently high energy and momentum transfer, neutron scattering from liquid helium can be expected to provide information about the momentum distribution $n(p)$ of individual helium atoms. While any experimental information about $n(p)$ for helium atoms is of interest, it is particularly important to obtain knowledge regarding the shape of $n(p)$ near $p = 0$. The shape of this part of the momentum spectrum bears on the question of the existence of a condensation in momentum space. Much of the theoretical basis for understanding superfluid He II involves the notion of macroscopic occupation of a

single quantum state: the zero-momentum state for an infinite system at rest. The existence of such a condensed mode, as a consequence of Bose-Einstein condensation, was first discussed quantitatively by Penrose and Onsager[1] following the early work of London.[2] For a system of noninteracting bosons, the condensate density $\rho_0(T)$ is expected to be the full fluid density at absolute zero, while for a real fluid like $^4$He, $\rho_0(T=0)$ is less than the total fluid density $\rho$. Recent theoretical estimates of $\rho_0/\rho$ at $T=0$ include those of Penrose and Onsage (0.08), McMillan[3] (0.11), Parry and Rathbone[4] (0.13–0.25), and Schiff and Verlet[5] (0.105).

Hohenberg and Platzman [6] have suggested the use of neutron inelastic scattering to detect the presence of a zero-momentum condensate in He II. The essence of their proposed approach is to measure the differential scattering cross sections for He II with sufficiently high-energy neutrons so that the neutron probe is sensitive to the motions of single helium atoms. For neutrons scattered from helium atoms in the zero-momentum state, the energy transferred from the neutron would be equal to the recoil energy, broadened by final-state interactions. For liquid-helium atoms not in the condensate, the energy transfer would be the recoil energy broadened by the Doppler shift. It has been estimated[6] that the Doppler broadening is several times as large as the broadening because of interparticle interactions on the recoiling helium atom. If this simple picture holds true, the neutron scattering cross sections are expected to be comprised of two components: a narrow one for scattering from condensate atoms with an area proportional to $\rho_0(T)$ and a wider distribution due to scattering from noncondensate atoms with an area proportional to $1-\rho_0(T)/\rho$. Qualitatively, Hohenberg and Platzman showed that this cross section would look like a small narrow peak superimposed on a large wider peak.

Although there have been a number of neutron scattering investigations of liquid helium, most of these have been directed toward measurement of the collective modes or the dispersion curve $\omega(\kappa)$ which for liquid helium is found to exist in the energy and momentum-transfer range 0– ~2 meV and 0– ~4 Å$^{-1}$, respectively. Recently, Cowley and Woods[7,8] have published the results of neutron scattering measurements on He I and He II, using momentum transfers of 2–9 Å$^{-1}$. At the higher values of $\kappa$ used in their work, the scattering appears to be close to free-particle scattering while at the lower-momentum transfers which they used, the measured energy transfers were somewhat less than those expected from the free recoil of single helium atoms. Cowley and Woods (CW) observed that the full width at half-height (FWHH) of their helium cross sections showed a marked temperature dependence near the $\lambda$ temperature. Further, they deduced that the observed width changes were consistent with a condensate fraction of $(17\pm10)\%$.

In the present work,[9] double-differential cross sections for neutron scattering from liquid $^4$He were obtained for much higher energy and momentum transfers than in previously reported studies. The free-particle excitation curve $\hbar\omega=\hbar^2\kappa^2/2m_{\mathrm{He}}$ was followed to $\hbar\omega$ and $\kappa$ values of 213 meV and 20.3 Å$^{-1}$, respectively. Measurements of double-differential cross sections were obtained for a range of helium temperatures 4.2–1.27 °K. The angular dependence of the total helium scattering is compared to that expected for free-particle scattering. A marked temperature dependence is observed in the shape of the double-differential cross section. This temperature dependence is interpreted in terms of the Hohenberg-Platzman[6] idea that there are two components in the cross section below $T_\lambda$, i.e., a normal and a condensate fraction.

## II. EXPERIMENTAL

All measurements of double-differential cross sections were made with the Battelle-Northwest Rotating Crystal and Chopper[10] time-of-flight spectrometer. Instrument resolution was optimized for the He scattering experiments by the addition of a 4-m flight path, which was installed at 154.3°, the largest available scattering angle. At this angle a freely recoiling helium atom carries off 62.5% of the initial neutron energy. Other scattered neutron detectors were located on 1.5-m flight paths at 14.5°, 29.6°, 44.5°, 59.5°, 90.5°, 121°, and 141° in the horizontal plane surrounding the liquid-helium sample. Time-of-flight (TOF) spectra were obtained simultaneously at all scattering angles. The TOF distributions were converted to double-differential cross sections with the aid of a large digital computer. Helium differential cross sections reported here were normalized[11] to a total scattering cross section of 0.724 b.

The liquid-helium scattering sample was contained in the tail of a liquid-helium Dewar which could be pumped to reduce the temperature to about 1.25 °K along the saturated vapor-pressure curve. A 4.0-cm-diam cylinder with aluminum walls of 0.076-cm thickness contained the neutron target, which was surrounded by a 0.076-cm-thick aluminum radiation shield at liquid-nitrogen temperature and an outer vacuum jacket of 0.165-cm-thick aluminum. About 5% of the incident neutron beam is scattered from the liquid-helium sample and about 6% from the metal parts of the cryostat tail. The sample-holder scattering is primarily elastic and therefore does not cover the energy range of the helium scattering peak at large scattering angles. A background measurement was made, for each set of operating conditions, without liquid helium in the Dewar tail, but with the tail and radiation shield maintained at

liquid-nitrogen temperature. Temperature determinations of the liquid-helium sample were made by measurements of the helium vapor pressure and by carbon resistance thermometers calibrated by pressure measurement prior to each experiment. Temperature was usually controlled by manual adjustment of valves in the pump lines and in some experiments with the aid of an automatically controlled heater inserted into the liquid helium. The temperature variation during a cross-section measurement averaged ± 1.5% from the nominal quoted temperatures.

The pulsed initial beam of monochromatic neutron was obtained from a rotating single crystal of aluminum 3.8 cm in diameter by 10 cm high. This monochromator was rotated, at 4500 rpm, about the [001] direction and was phased with the coarse chopper to produce four monochromatic bursts per revolution from either the (220) or the (200) planes. Collimator angles ($\Delta\theta_c$) of 0.139° and 0.079° were used. The initial neutron energies ($E_1$) of 171.5 and 343 meV were determined by TOF measurement in the unscattered beam. Energy resolutions for neutrons scattered 154.3° and corresponding to the center of the helium cross-section peaks are given in Table I. The instrumental resolution width is about equal to the sharpest structure expected in the scattering cross section, i.e., the scattering from the condensate atoms. Theoretical[6] estimates of condensate peak widths are also given in Table I. Cross sections measured with the 4-m flight path at 154.3° were used in detailed analysis of shapes since the energy resolution for the shorter flight paths was generally inadequate to clearly resolve any structure which might be expected from a zero-momentum condensate.

### III. EXPERIMENTAL RESULTS

A total of 11 neutron scattering experiments were carried out with $E_1 = 171.5$ meV, over the temperature range 1.26 °K to $T_\lambda$ and another eight experiments in the range $T_\lambda$ to 4.20 °K. At initial energies of 343 meV, one experiment was run at 4.20 °K and another at 1.28 °K. Figure 1 presents typical cross-section results for helium scattering measurements. This figure includes $d^2\sigma/d\Omega dE$ curves for $E_1 = 171.5$ meV at 1.28 ± 0.01 °K and similar results for $E_1 = 343$ meV at $T = 1.28 \pm 0.02$ °K. Calculated instrumental resolution is shown by the heavy bars in the cross-section peaks. The stepped shape of the data points at small scattering angle is the result of choosing time and energy channel widths to optimize the presentation for the large-scattering-angle detectors. The arrows above the cross-section peaks indicate the energy transfer associated with a freely recoiling helium atom.

TABLE I. Instrumental energy resolution FWHM $\Delta E_2$ for neutrons scattered from liquid helium at 154.3° and the estimated width of the $\rho_o$ peak $\Delta E_c$ at constant momentum transfer, for different values of initial energy $E_1$ and collimator angles $\Delta\theta_c$, used in the helium cross-section measurements. The error on $E_1$ gives only the Bragg uncertainty in the unscattered beam.

| $E_1$ (meV) | $\Delta\theta_c$ (deg) | $E_2$ (meV) | $\Delta E_2$ (meV) | $\Delta E_c$ |
|---|---|---|---|---|
| 171.5 ± 3.4 | 0.139 | 64.3 | 4.65 | 6.0 |
| 171.5 ± 1.9 | 0.079 | 64.3 | 3.4 | 6.0 |
| 343.0 ± 6.8 | 0.139 | 128.5 | 9.2 | 8.4 |

Table II gives the energy and momentum transfers expected for free-particle scattering and the actual average of 15 measured energy transfers found from the position of the midpoints of the cross-section peaks taken at half-height. The measured recoil energies obtained in this way cannot be compared directly with the calculated results because the measurement is made at constant scattering angle $\Theta$ and not constant momentum transfer. Therefore, an adjusted set of experimental recoil energies is also presented in Table II. This adjustment was made by determining the shift, in $\omega$, of the centroid position of a simple Gaussian-shaped $S(\kappa,\omega)$ at constant $\kappa$, when this $S(\kappa,\omega)$ is converted to a constant $\Theta$ cross-section representation. The shift determined in this way is ~0.6% for the He cross sections at $\Theta = 154.3°$. It will be shown that a Gaussian in $\omega$ at constant $\kappa$ gives a good model for the helium scattering discussed here. For $E_1 = 171.5$ meV, the adjusted experimental values are well within their standard deviations of the calculated values. The adjusted values for $E_1 = 343$ meV also lie within one standard deviation of the theoretical recoil energies. Errors assigned to the measured values of $\hbar\omega$ include uncertainties in the measurement of $E_1$ and $E_2$ as well as the uncertainty in the determination of the midpoints of the scattering peaks. A shift in the peak position of $S(\kappa,\omega)$ has been inferred by Sears[12] from his treatment of high-energy neutron scattering from liquid helium, which includes the effect of final-state interactions. The predicted theoretical shift is 25 °K or about 2.25 meV. The present experimental value of $\hbar\omega$, for the 154.3° counter, is 0.5 ± 0.8 meV lower than the free recoil energy. The experimental error is believed to be conservative. Therefore, it is unlikely that the measured $\hbar\omega$ differs from the free-atom value by as much as 2.25 meV.

Figure 2 indicates the locations, in $\kappa$ and $\hbar\omega$, of the present measurements on the free-particle excitation curve for $^4$He. This figure also shows the range of $\kappa$ covered in the experiments of Cowley and Woods.[7,8] Their results extend from the region near the end of the phonon-roton dispersion curve to $\kappa \simeq 9$ Å$^{-1}$. At the lower values of $\kappa$, the CW values

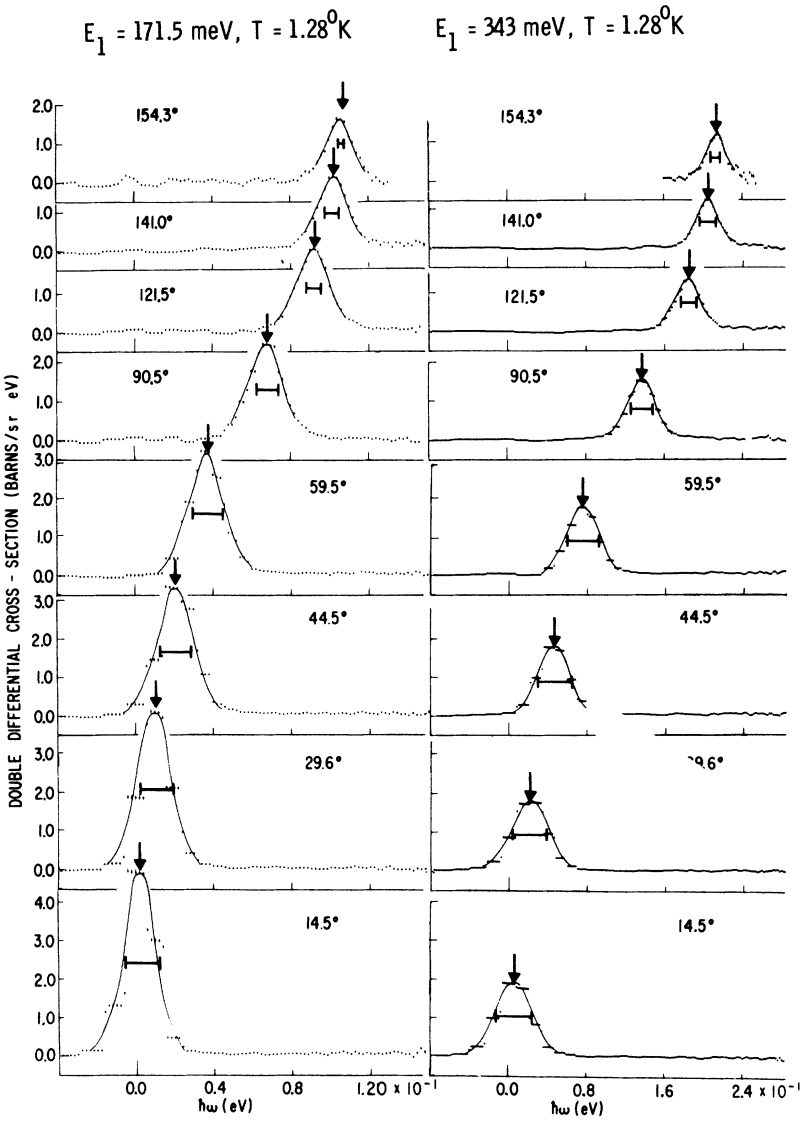


FIG. 1. Double-differential cross sections for liquid He II at 1.28°K. Calculated instrumental resolutions FWHM are shown as bars inside the scattering peaks. Arrows placed above the scattering peaks indicate the energy transfers expected for free recoil of the helium atoms. Smooth lines have been drawn through the cross-section points to improve the visual presentation.

lie somewhat below the free-particle curve, approaching close to the free-particle curve in the $\kappa$ range 7–9 $\text{Å}^{-1}$. Small deviations from free-particle recoil energies at low values of $\kappa$ probably would not be evident in the present results because of the inadequate energy resolution on $\hbar\omega$ in the appropriate range 2–10 meV, with the high initial neutron energies of 171.5 and 343 meV which were used. The CW measurements would seem to place the onset of the quasi-free-particle-scattering region at $\kappa$ values approximately $\frac{1}{2}$–$\frac{1}{3}$ those used for the 154.3° detector bank in the present research.

The double-differential cross sections have been integrated over energy for each detector scattering angle to give the single-differential cross section $d\sigma/d\Omega = \sigma(\Theta)$. Mean values for $\sigma(\Theta)$ were obtained by averaging the results of 13 separate experiments with $E_1 = 171.5$ meV and two experiments with $E_1 = 343$ meV. These mean values are plotted in Fig. 3. Standard errors on the mean are shown by error bars for the $E_1 = 171.5$ meV results only. Also shown in Fig. 3 is the theoretical curve of the cross section, see Eq. (1), for elastic free-particle scattering[13]:

$$\frac{d\sigma}{d\Omega} = \frac{\sigma_f}{2\pi}\frac{A+1}{A}\left(\frac{E_2}{E_1}\right)^{1/2}\frac{1}{1+(A-1)/(A+1)E_1/E_2}\,, \tag{1}$$

where $\sigma_f$ is the free-atom cross section, 0.724 b was used for $\sigma_f$, $A$ is the ratio of the $^4$He mass to the neutron mass, $E_1$ and $E_2$ are the initial and final neutron energies, respectively. There is good agreement between the theoretical free-particle

TABLE II. Energy and momentum-transfer data for helium scattering peaks. Measured values are given for the center of a line bisecting the cross-section peaks at half-height. Calculated energies and $\kappa$ values are also tabulated for freely recoiling He atoms at the various scattering angles $\Theta$. Adjusted measured values are corrected for peak symmetry, see text. Errors are total experimental uncertainties.

| | $E_1 = 171.5$ meV | | | | $E_1 = 343$ meV | | | |
|---|---|---|---|---|---|---|---|---|
| $\Theta$ (Deg) | $\kappa$ (Å$^{-1}$) | $\hbar\omega$ (meV) Meas. | Adj. meas. | Calc. | $\kappa$ (Å$^{-1}$) | $\hbar\omega$ (meV) Meas. | Adj. meas. | Calc. |
| 154.3 | 14.33 | 106.0 ± 0.8 | 106.65 ± 0.8 | 107.15 | 20.26 | 213.0 ± 1.6 | 214.0 ± 1.6 | 214.30 |
| 141.0 | 14.04 | 101.5 ± 0.7 | 102.1 ± 0.7 | 102.86 | 19.86 | 204.8 ± 1.3 | 205.8 ± 1.3 | 205.82 |
| 121.0 | 13.35 | 91.7 ± 0.7 | 92.3 ± 0.7 | 93.09 | 18.88 | 184.5 ± 1.4 | 185.6 ± 1.4 | 186.18 |
| 90.5 | 11.54 | 68.1 ± 0.8 | 68.5 ± 0.8 | 69.50 | 16.31 | 137.5 ± 1.6 | 138.3 ± 1.6 | 139.00 |
| 59.6 | 8.56 | 37.8 ± 1.0 | 38.0 ± 1.0 | 38.25 | 12.10 | 74.8 ± 1.9 | 75.3 ± 1.9 | 76.50 |
| 44.5 | 6.67 | 22.5 ± 1.1 | 22.6 ± 1.1 | 23.27 | 9.44 | 45.3 ± 2.0 | 45.6 ± 2.0 | 46.54 |
| 29.6 | 4.58 | 10.7 ± 1.2 | 10.8 ± 1.2 | 10.98 | 6.48 | 21.5 ± 2.2 | 21.6 ± 2.2 | 21.96 |
| 14.5 | 2.29 | 2.7 ± 1.3 | 2.7 ± 1.3 | 2.74 | 3.23 | 4.3 | 4.3 | 5.48 |

cross-section curve and the experimental points for $E_1 = 171.5$ meV at all detector angles except 14.5°. The $\kappa$ value for 14.5° corresponds to the region of the large peak in the helium structure factor,[14] $S(\kappa)$, at $\kappa \simeq 2$ Å$^{-1}$, which is related to coherent effects in the scattering. The deviation above the free-particle cross section, for the 14.5° point, is approximately the same magnitude as the corresponding deviation of $S(\kappa)$ above its limiting value at high $\kappa$, i.e., $S(\kappa) = 1$. Similar good agreement exists between the experimental cross sections for $E_1 = 343$ meV. In this case, the peaking in $S(\kappa)$ cannot be seen, since $\kappa$ is already 3.2 Å$^{-1}$ at the smallest detector angle, i.e., 14.5°. These results provide additional evidence for believing that at the higher $\kappa$ values used in the present experiments the neutron probe is sensitive only to the single-helium-particle motions.

Detailed information concerning the momentum distribution of single helium atoms can best be inferred from the present measurements at 154.3°

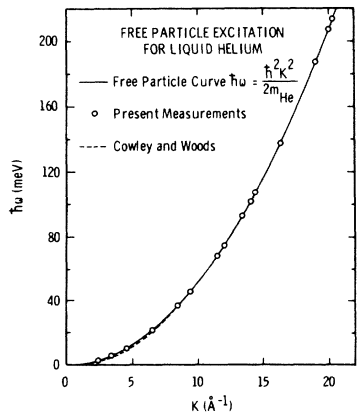


FIG. 2. Free-particle excitation curve for $^4$He. Regions investigated in previous studies by Cowley and Woods (Ref. 8) and in the present work are indicated.

scattering angle where the highest instrumental resolution was available. Figures 4 and 5 present some of the double-differential cross sections for $E_1 = 171.5$ meV measured at this angle for a range of temperatures. Several independent scattering experiments were usually carried out at each helium temperature; reproducibility was generally within the experimental errors indicating a high degree of consistency in the cross-section measurements. An instrumental resolution of ~4.65 meV on $E_2$ was used for all measurements at this energy except for the run at 4.185 °K and the one at 1.275 °K which were obtained using a calculated resolution of ~3.4 meV for neutrons scattered near the centroid of the helium cross-section peak. No significant difference is observed by visual examination of the shapes of the cross sections for these two resolutions. The shapes of the differential cross sections do, however, exhibit a temperature dependence. There is a narrowing of the width of the cross-section peak as the temperature decreases from 4.2 °K to $T_\lambda$. Below $T_\lambda$ there is also a gradual change in the shape of the cross-section peak. While above $T_\lambda$ the cross section is relatively Gaussian (a slightly skewed Gaussian gives a good fit to the cross section), below $T_\lambda$ the shape becomes more pointed and a single Gaussian will not fit the peak as well. Figure 6 presents the double-differential cross-section results for $E_1 = 343$ meV, and $\Theta = 154.3°$. Measurements were obtained at two temperatures 4.2 and 1.28 °K for this initial energy. Smooth curves were fitted by eye to the data points in order to make the shape differences more apparent. No attempt was made to normalize the areas under the cross-section curves at $\Theta = 154.3°$ to a constant value. It is apparent in Fig. 6 that there is a substantial difference in areas under the 4.2 and 1.28 °K curves. This difference is about 24% and is by far the largest difference observed for any of the cross-section measurements. Typically, the areas under the

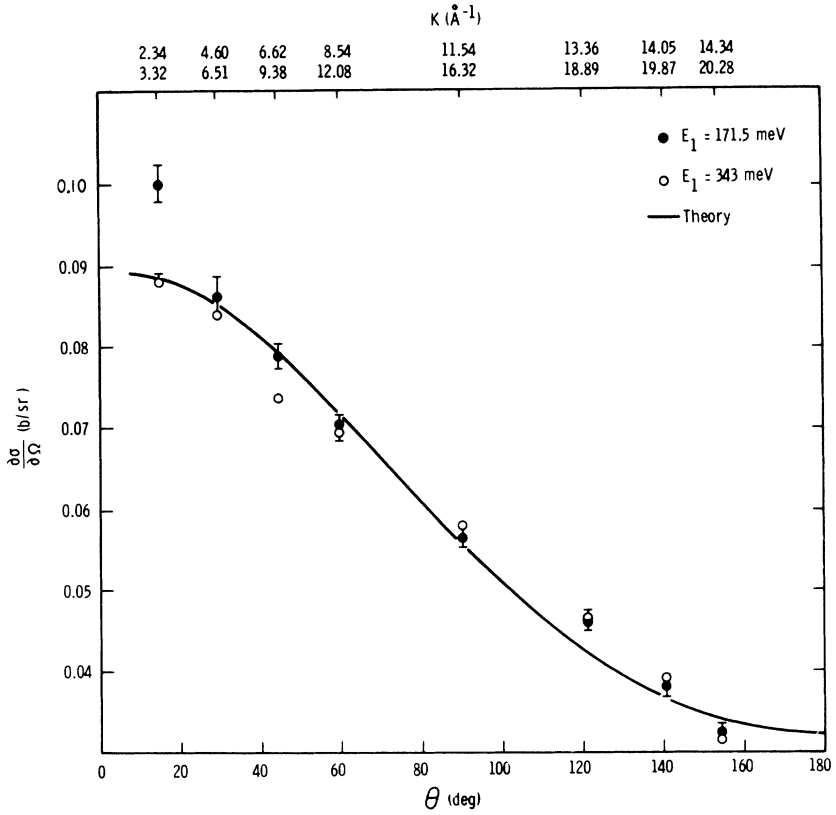


FIG. 3. Experimental values of the single-differential cross section compared to the theoretical cross section for elastic free-particle scattering. The upper $\kappa$ scale is for $E_1 = 171.5$ meV and the lower $\kappa$ scale for $E_1 = 343$ meV.

cross-section curves shown in Figs. 4 and 5 are in agreement to within better than 10%. At other angles, where signal-to-noise ratio is better because of the shorter flight path, the areas under the cross-section curves for $E_1 = 343$ meV agree to within several percent for the two temperatures used. Difficulties in making exact background subtractions are believed to be the main contributors to the variations observed in the single-differential cross sections for the long-flight-path detector. The background, however, is quite smooth and errors in normalization are not expected to influence any structure which might be found near the top of a helium scattering peak.

The full widths at half-maximum (FWHM) of the differential cross-section peaks at 154.3° are plotted in Fig. 7. Each point represents the resolution unfolded FWHM for a separate cross-section measurement. A definite change in slope occurs, in the width data, as the phase transition is traversed. This is emphasized by the straight-line segments which were least-squares fitted to the data above and below $T_\lambda$. A change in the slope of the $\Delta E$-vs-$T$ data, as $T$ decreases below $T_\lambda$, suggests a transition which could be associated with the growth of an additional component in the cross sections, e.g., a narrow condensate fraction. A knee in the widths of the scattering peaks similar to that in Fig. 7 has also been observed by CW.[7,8]

For neutrons which scatter off free atoms, the scattered neutron peaks are Gaussians in $\hbar\omega$ at constant $\kappa$ and peak widths are proportional to the square root of the kinetic energy of the scattering atoms. The kinetic energy for liquid-helium atoms as a function of temperature can be obtained by applying phase equilibria criteria to the liquid and its saturated vapor. The Gibbs free energy as well as the temperature and pressure of liquid and vapor are equal along the *svp* curve. Therefore,

$$G_l = G_v \quad , \tag{2}$$

$$U_l = U_v + P(V_v - V_l) - T(S_v - S_l) \quad , \tag{3}$$

$$K(T)/N = -P(T)/N - L_v + \tfrac{5}{2}kT - PV_l \quad , \tag{4}$$

where $K(T)/N$ and $P(T)/N$ are the average kinetic and potential energies per liquid-helium atom, $L_v$ is the latent heat of vaporization, $k$ is Boltzmann's constant, $T$ and $P$ are the absolute temperatures and pressures, and $V_l$ is the volume per liquid-helium atom. Equation (4) is obtained from Eq. (3) under the assumption that the saturated helium vapor can be treated as an ideal gas. The last three terms in Eq. (4) are easily obtained from known experimental data. The potential-energy term can be computed from an integral of the pair potential $V(r)$ over the radial distribution function $g(r)$:

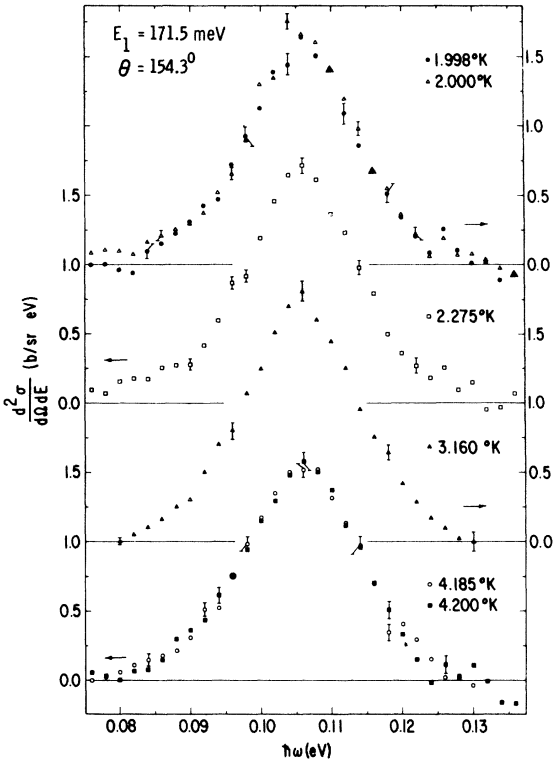


FIG. 4. Double-differential cross section at $\Theta = 154.3°$, $E_1 = 171.5$ meV and a range of helium temperatures.

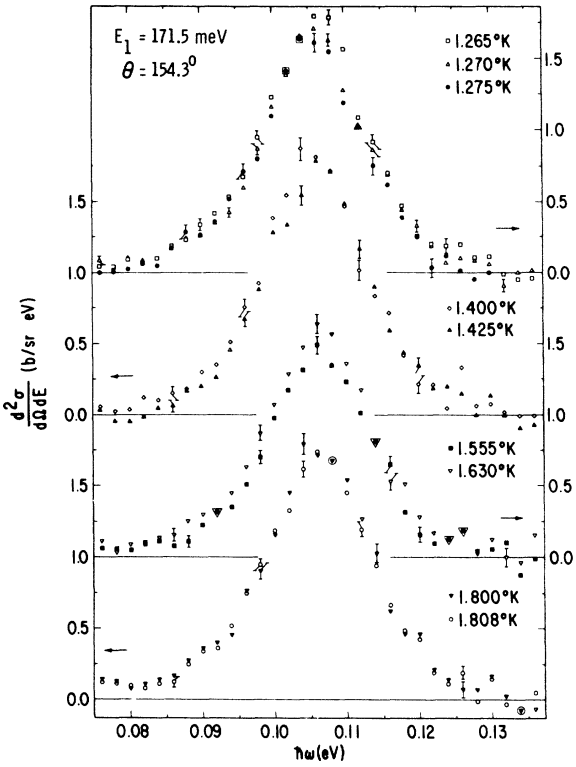


FIG. 5. Double-differential cross section at $\Theta = 154.3°$, $E_1 = 171.5$ meV and a range of helium temperatures.

$$\frac{P}{N} = \tfrac{1}{2}\rho \int_0^\infty V(r)\, g(r)\, 4\pi r^2 dr \quad . \tag{5}$$

Information on the radial distribution function is available at several temperatures from x-ray and neutron scattering studies.

If we assume a free-particle model for the neutron scattering and, furthermore, that only one component or one type of liquid-helium atom contributes to the scattering, then the widths of the measured peaks are expected to be proportional to $(K/N)^{1/2}$. Under these assumptions the measured widths in Fig. 7 should exhibit the same temperature dependence as $(K/N)^{1/2}$ when this quantity is obtained from Eq. (4). The temperature dependence of the widths, computed from Eq. (4), using values of latent heat, pressure, and density from Ref. 14, is shown in Fig. 7 for comparison with the measured scattering peak widths. In the computation, a potential energy of $-180$ J/mole was used at $T = 0$. At finite temperatures, the PE was assumed to vary with the ratio of the macroscopic fluid density at finite temperature, to the density at 0 °K. Calculations,[15] using Eq. (5) with several reasonable pair potentials and experimental values for the radial distribution[16,17] function obtained at several fluid densities, indicate that the assumed temperature variation of the PE constitutes a good approximation. The assumed temperature variation of PE is also in good agreement with the dependence of PE on $T$ found by Goldstein and Reekie.[18] The computed widths have been normalized to agree with the measured widths at 2.8 °K. This temperature corre-

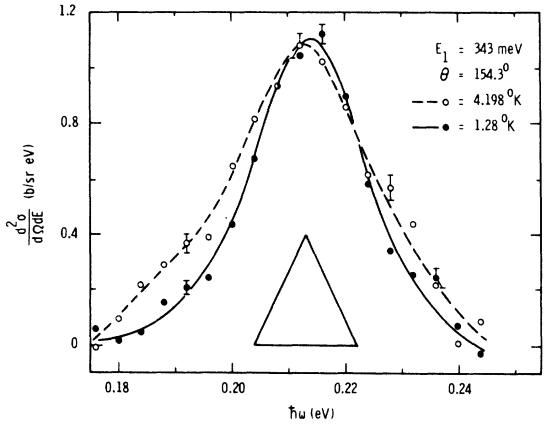


FIG. 6. Double-differential cross sections at $\Theta = 154.3°$, $E_1 = 343$ meV for liquid He at 4.19 and 1.28 °K. The instrumental resolution FWHM is indicated by the FWHM of the resolution triangle.

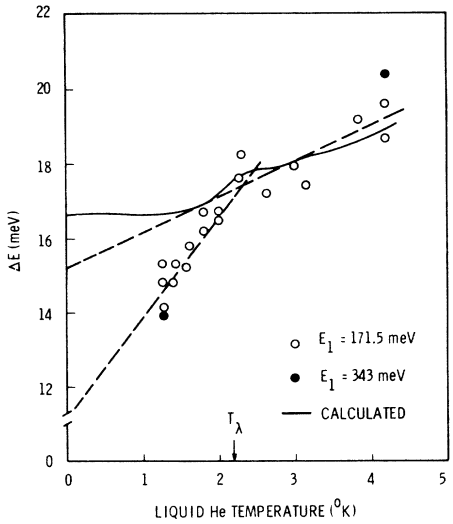


FIG. 7. Full width at half-maximum versus temperature for the neutron scattering peaks $\Theta = 154.3°$. Hollow circles are for $E = 171.5$ meV experiments, solid circles represent energy widths for $E_1 = 343$ meV which have been adjusted for the higher $\kappa$ used by dividing the measured widths by $\sqrt{2}$. This figure also shows the temperature dependence of the widths which have been computed from Eq. (4).

sponds to the midpoint of the experimental temperature range. Both measured and computed results are in good agreement for $T > T_\lambda$. Below $T_\lambda$, however, the measured widths are narrower than those calculated from Eq. (4). Such a narrowing of the FWHM would be consistent with the expected peak shapes if a fraction of the helium atoms are condensed into a zero-momentum condensate.

More detailed information concerning the temperature dependence of the neutron cross sections can be obtained by comparing the entire shape of the scattered neutron spectra for measurements above and below the $\lambda$ point. Figure 8 presents typical raw TOF scattered neutron spectra for helium temperatures of 4.2 and 1.27 °K with an initial energy of 171.5 meV. Instrumental resolution is indicated by the bar inside the scattering peaks. A flat background has been subtracted and the areas under both TOF peaks have been made equal to facilitate comparison of shapes. The data in Fig. 8 have not been smoothed except that time channels have been summed in pairs. Visual examination of Fig. 8 indicates that the helium peak at 1.27 °K is considerably narrower at half-height and generally sharper near the center than the 4.2 °K peak. Analog-computer analysis of the shapes of the double-differential cross sections, derived from data like that shown in Fig. 8, indicates that a single skewed Gaussian, in energy, provides a good fit to the scattering peaks above $T_\lambda$. However, at helium temperatures near 1.27 °K, a single component of this type does not provide as good a fit to the experimental results even though the width is varied to account for changes in the sample temperature. The fit fails primarily in the upper part of the peaks where scattering from a condensate component would be expected to contribute. Addition of a second narrow component whose width is assigned according to the Hohenberg and Platzman[6] estimate of the condensate width, permits a better fit to be made to the cross sections below $T_\lambda$. However, a well-resolved two-component scattering peak, such as that suggested in Ref. 6, is not observed in the present experimental results. Structure in the scattering peaks is of a subtler nature and requires careful analysis to determine what contribution to the scattering may be related to a momentum condensate.

## IV. COMPARISON OF EXPERIMENT WITH THEORY

A theoretical model for neutron–liquid-helium scattering, at high-momentum transfer, has been developed by Puff and Tenn.[19] This model assumes the scattering law $S(\kappa, \omega)$ is Gaussian in $\hbar\omega$ at constant $\kappa$ and centered on the free-particle recoil energy. With this assumption, and the use of certain sum rules, a model results which involves only two parameters: the average kinetic energy per particle $K/N$ which is related to the width of $S(\kappa, \omega)$, and the fractional condensate density $\rho_0/\rho$. Use of such a model seems justified by the observation of helium recoil energies which lie on the free-particle excitation curve, the good agreement between the measured single-differential cross sections and the theoretical cross section for free-particle scattering, and by the observation that the measured cross sections at $T > T_\lambda$ can be well fitted by a theo-

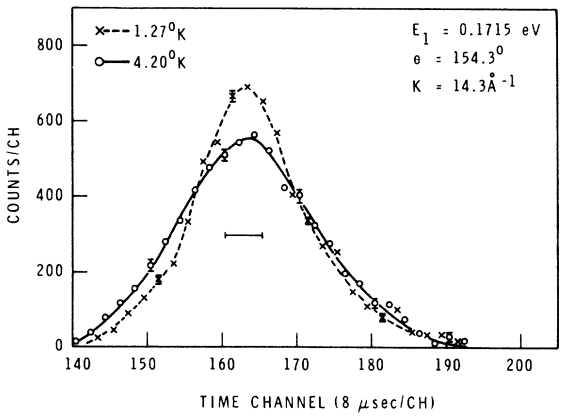


FIG. 8. Raw TOF scattering data for liquid helium at 4.20 and 1.27 °K. Backgrounds have been subtracted and areas under both peaks have been made equal. The instrumental resolution FWHM is represented by the bar near the middle of the peaks.

retical cross section derived from an $S(\kappa,\omega)$ which is a single simple Gaussian at constant $\kappa$.

Equation (6) gives the Puff-Tenn (PT) result used for comparison with experiment:

$$\frac{d^2\sigma}{d\Omega dE_2} = \frac{\sigma_b}{8\pi^2\hbar}\left(\frac{E_2}{E_1}\right)^{1/2}\left[\frac{2\rho_0}{\rho}\left(\frac{\pi}{\Gamma_1(\kappa)}\right)^{1/2}(e^{-\Gamma_1^{-1}(\hbar\omega-\hbar\omega_0)^2}) + 2\left(1-\frac{\rho_0}{\rho}\right)\left(\frac{\pi}{\Gamma_2(\kappa)}\right)^{1/2}(e^{-\Gamma_2^{-1}(\hbar\omega-\hbar\omega_0)^2})\right]. \quad (6)$$

In this expression $\sigma_b$ is the bound-atom cross section for $^4$He which was set equal to 1.13 b, $\rho_0/\rho$ is the fractional condensate density, $E_1$ and $E_2$ are the initial and final neutron energies, respectively, $\hbar\omega_0(\kappa)$ is the recoil energy which is a function of $\kappa$ and therefore not a constant for constant scattering angle. The expression for the cross section has two parts: The first part, involving a Gaussian with a width $(\Gamma_1)^{1/2}$, is identified with scattering from helium atoms in the condensate, while the second Gaussian, with width $(\Gamma_2)^{1/2}$, is the scattering expected from the uncondensed or normal helium atoms. From Ref. 6, the width of the condensate peak $(\Gamma_1)^{1/2}$ is estimated by

$$\Gamma_1(\kappa) = \frac{1}{4\ln 2}\left(\frac{\rho\sigma\kappa}{M_{\mathrm{He}}}\hbar^2\right)^2 , \quad (7)$$

where $\rho$ is the liquid-helium atom density, $\sigma$ is the He-He scattering cross section for which one can use[6] $2\times10^{-15}$ cm$^2$ for the $\kappa$ range of interest, $\hbar\kappa$ is the momentum transfer, and $M_{\mathrm{He}}$ is the mass of a helium atom. The width of the Gaussian associated with the uncondensed helium atoms is defined by the PT model in such a way that it involves both the average kinetic energy per He atom $K/N$ and the fractional condensate density $\rho_0/\rho$:

$$\Gamma_2(\kappa) = [\tfrac{8}{3}(K/N)\hbar\omega_0 - (\rho_0/\rho)\Gamma_1]/(1-\rho_0/\rho). \quad (8)$$

The cross-section expression, Eq. (6), was least squares fitted to the experimental results with aid of computer program LIKELY.[20] A total of 19 separate experiments with $E_1 = 171.5$ meV were fitted by varying the PT-model parameters. Only the scattering peaks at $\Theta = 154.3°$ were used for this detailed analysis. Experimental resolution was taken into account by convoluting the theoretical cross section with a resolution function of the form

$$(\pi\Gamma_R)^{-1/2}\exp[-\Gamma_R^{-1/2}(\hbar\omega-\hbar\omega')]^2 ,$$

where

$$\Gamma_R = \Gamma_R(\hbar\omega') = \frac{1}{4\ln 2}(\Delta E_2)^2 ,$$

and $\Delta E_2$ is the instrumental resolution.

The theory-experiment comparison was made with double-differential cross sections which were computed from the raw TOF data on a channel-by-channel basis. This procedure results in minimum perturbation to any structure which is present in the raw data and ensures that the statistical errors calculated for each cross-section point are uncorrelated. Use of uncorrelated errors is a necessary requirement for the statistical analysis which is discussed below.

The result of least-squares fitting the theoretical cross section to a measured scattering peak, for 4.20 °K liquid helium, is shown in the left-hand

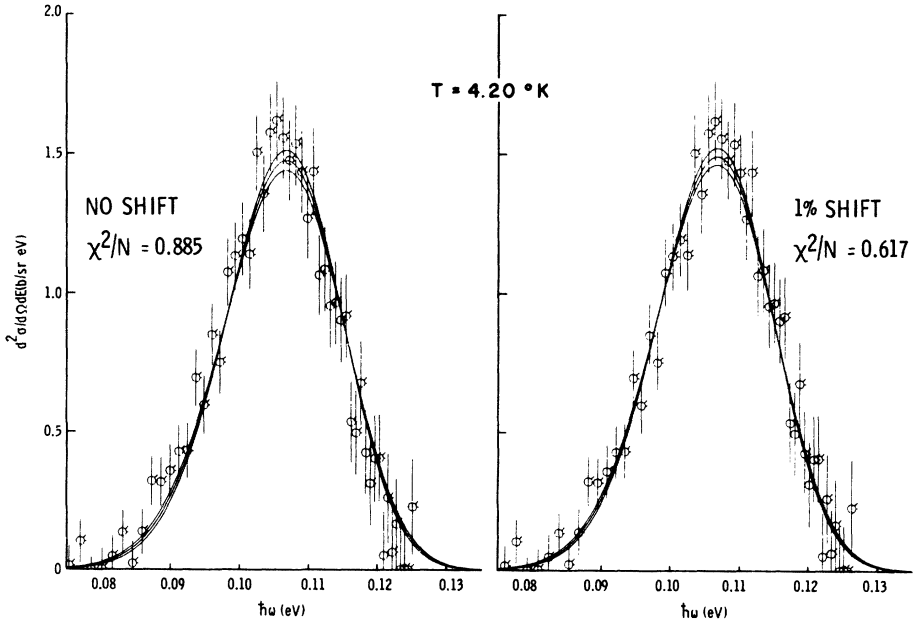


FIG. 9. Least-squares fits of one-parameter PT theory to a scattering peak at 4.20 °K. Data in the left-hand part of figure have been shifted toward higher $\hbar\omega$ by ~1%. Values obtained for the fitting parameter, $K/N$, are 14.57 ± 0.77 and 14.22 ± 0.64 °K, respectively, for the unshifted and shifted data. The initial energy $E_1 = 171.5$ meV, $\Theta = 154.3°$, and $\kappa$ at the peak centroid is 14.3 Å$^{-1}$.

part of Fig. 9. For this fitting, the condensate fraction in Eq. (6) was set equal to zero and, therefore, the theoretical cross section is a single Gaussian in $\hbar\omega$ at constant $\kappa$ which is fitted by varying one free parameter, i.e., the $K/N$. Equation (6) in this form is identical to the scattering function for free gas atoms. In the fitting process, the area under the theoretical peak is normalized to the area under the experimental scattering peak, and this procedure is followed in all theory-experiment comparisons which are made here. Three continuous curves are drawn by the computer to indicate the least-squares fit. The central curve is the actual least-squares fit while the two adjacent curves represent one rms deviation of the fitted curve. From a visual examination of the left-hand part of Fig. 9, it is apparent that a better fit could be obtained by slightly shifting either the theory curve to lower $\hbar\omega$ or the experimental data points to higher $\hbar\omega$. The right-hand side of Fig. 9 presents the result for a least-squares fit of the one-parameter theory to the data points after the experimental energy scale has been shifted 1% towards higher $\hbar\omega$. A shift of the scattering peaks, toward energies lower than the free-particle recoil energies, would not be surprising since the known interactions between the liquid-helium particles can be considered to cause an increase in the effective mass of the scattering atoms. However, a shift of 1% in $\hbar\omega$ is not sufficiently large to place it out of the measurement uncertainty. The $\chi^2/N$ values[21] are 0.885 and 0.617, with $N = 53$ for the unshifted and shifted data, respectively. Similar improvements in fit are found at all helium temperatures when the experimental energy scale is shifted slightly toward higher energy transfers. The optimum shift is found to be ~1 meV or ~1% for the $E_1 = 171.5$ meV experiments. Since the experimental error on the determination of $\hbar\omega$, see Table II, is just in this range, it is difficult to conclude where the shift originates and it could, in fact, be due to a combination of a small deficiency in the theory and a small systematic error in the experimental energy scale. In the following analysis, results will be presented, for $E_1 = 171.5$ meV, both for data which have not been shifted in any way and for data which have been shifted ~1 meV or 1% by multiplying the $\hbar\omega$ scale by a suitable factor. Conceptually, this shift may be thought of as a change in the energy scale within the experimental uncertainties and not as a change in the PT model. Least-squares fitting of theory to experiment in the case of the $E_1 = 343$ meV data indicates no significant improvements in fit are obtained by shifting the data in the range 0–2 meV. Results for $E_1 = 343$ meV are therefore reported for unshifted data only.

Figure 10 presents the results of a least-squares fit of the PT theory to a scattering peak obtained

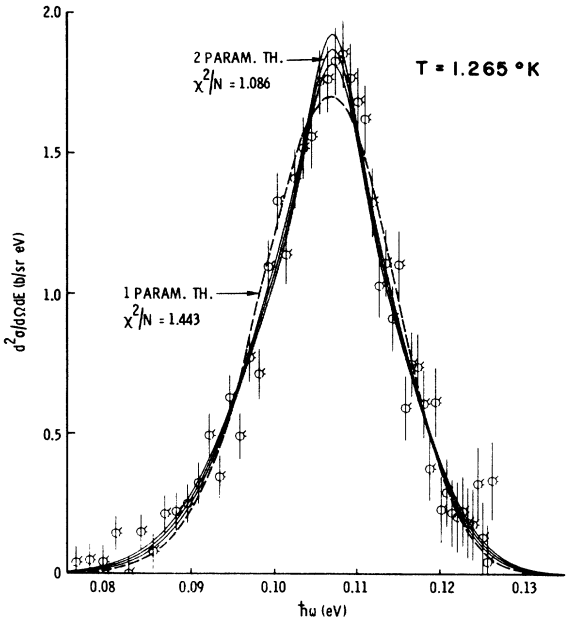


FIG. 10. Results of least-squares fitting the two-parameter and the one-parameter PT theory to neutron scattering data for liquid helium at 1.265 °K. Values obtained for the fitting parameters are $\rho_o/\rho = (9.4 \pm 2.1)\%$, $K/N = 13.9 \pm 0.8$ °K for the two-parameter theory and $K/N = 12.7 \pm 0.7$ °K for the one-parameter theory. The data have been shifted to higher $\hbar\omega$ by 1%.

for 1.265 °K liquid helium with $E_1 = 171.5$ meV and mean $\kappa = 14.3$ Å$^{-1}$. The experimental energy scale has been shifted 1% toward higher $\hbar\omega$. The three continuous curves are the least-squares fit for the two-parameter theory, i.e., where both $\rho_0/\rho$ and $K/N$ are varied to minimize $\chi^2$. For comparison, the fit to the one-parameter theory is also shown as a dashed line. From a visual examination one could conclude that both theories give satisfactory over-all fits to the data. However, the $\chi^2/N$ value, which is a measure of the goodness of fit, is substantially lower for the two-parameter theory. The probability obtained from the standard $\chi^2$ tables, that these $\chi^2$'s are due to statistical fluctuations alone, is 31 and ~2%, respectively, for the two- and one-parameter fits. It is worth mentioning that the sensitivity of the $\chi^2$ test depends on the assumption that the errors are due to counting statistics and do not include systematic components. The improvement in fit of the two- vs one-parameter theory in Fig. 10 is evident primarily in the extreme peak at the half-height point and in the tails of the scattering peak. The amount of improvement in fit is not dramatic when judged, e.g., on the basis of the size of a single error bar. However, the same type of improvements in fit are noted for all three of the scattering experiments with $E_1 = 171.5$ meV and $T \simeq 1.28$ °K. It should also be

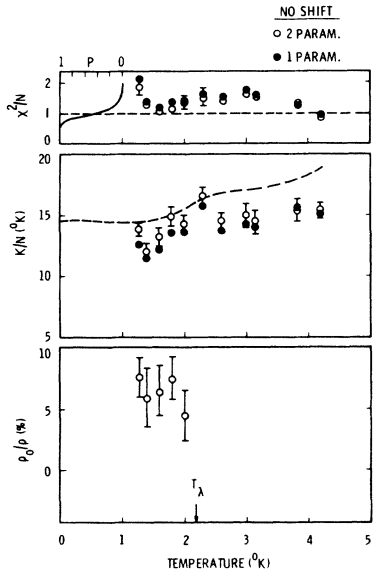


FIG. 11. Summary of results for $\rho_o/\rho$, $K/N$, and $\chi^2/N$ obtained from least-squares fits to the unshifted scattering peaks. The kinetic energy computed with Eq. (4) is shown as a dashed line. $E_1 = 171.5$ meV and $\Theta = 154.3°$.

mentioned that dramatic differences in shape due to a small fractional condensate density cannot, in our opinion, be expected because of the experimental resolution function, the relative widths expected for the condensate peak and the observed gross widths of the experimental scattering peaks, and the statistical variability on the data points.

Another statistical test, the $F$-ratio test, can also be used to compare fits. The $F$ ratio is given by $F_{1,N} = (\chi_1^2 - \chi_2^2)/(\chi_1^2/N)$, where $\chi_1^2$ and $\chi_2^2$ are obtained from least-squares fits of the one- and two-parameter theory to the same set of data. The statistic $F_{1,N}$ will be distributed as an $F$ variable, where $F$ is defined as the ratio of independent $\chi^2$'s, and the probability point on the $F$ distribution corresponding to the computed $F_{1,N}$ gives the probability that the one-parameter theory gives as good a fit to the data as the two-parameter theory. The computed value of the $F$ ratio for Fig. 10 indicates that the one-parameter theory would give as good a fit as the two-parameter theory only about 1 time in 1000 on a purely chance basis. This is evidence for choosing the two-parameter theory as a better model in this case.

Figures 9 and 10, and the associated discussion, have served to introduce the type of analysis which has been carried out on all the cross-section peaks. Conclusions obtained from the present theory-experiment comparison are best based upon the summary of results presented and discussed below. Figures 11 and 12 present values for the fitting parameters obtained from the least-squares fits of the one- and two-parameter versions of the PT theory to the helium scattering peaks, measured with $E_1 = 171.5$ meV at helium temperatures of 4.2–1.27 °K. Results are shown for unshifted data, Fig. 11, and data which have been shifted 1% toward higher $\hbar\omega$, Fig. 12. Nineteen separate scattering experiments with $E_1 = 171.5$ meV, $\Theta = 154.3°$, and mean $\kappa = 14.3$ Å$^{-1}$ were fitted with the one- and two-parameter versions of the PT theory. The results represent averages from three experiments at 1.27 °K and two experiments at 1.4, 1.6, 1.8, 2.0, 2.3, and 4.2 °K. Data from only one experiment were available at 3.83, 3.16, 3.00, and 2.62 °K. Error bars on the parameters are the standard deviations on the fitting parameters obtained from the least-squares fitting analysis by program LIKELY.[20] These errors are a function of the remaining variability between the data and the theory after the least-squares fits have been made.

While use of a two-component cross section, i.e., one which includes a zero-momentum condensate, is physically unsound at $T > T_\lambda$, this type of analysis does investigate the sensitivity of the model-experiment comparison. If, for example, the two- and one-component models fit the data equally well at $T < T_\lambda$, then there has been no evidence obtained for existence of a condensate in this model-experiment comparison. Conversely, a better fit to the data when using the two-component theory, as opposed to the one-component theory, at $T < T_\lambda$ and equally good fits at $T > T_\lambda$ would constitute evidence for a condensate fraction. As a measure of goodness of fit, we will examine the $\chi^2/N$ values which are given at the top of Figs. 11 and 12. A curve of statistical

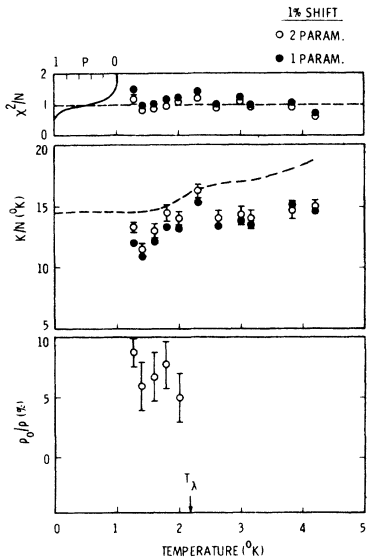


FIG. 12. Same results as for Fig. 11 except that the data are shifted 1% toward higher $\hbar\omega$.

TABLE III. Summary of results obtained from the $F$ test for groups of data in certain temperature ranges.

| | | Geom. mean prob. |
|---|---|---|
| Unshifted data | $T > T_\lambda$ | 0.123 |
| | $T > 2.62\,^\circ$K | 0.322 |
| | $T < T_\lambda$ | 0.0127 |
| Data shifted 1% | $T > T_\lambda$ | 0.0422 |
| | $T > 2.62\,^\circ$K | 0.211 |
| | $T < T_\lambda$ | 0.0055 |

probability vs $\chi^2/N$ for ~50 degrees of freedom is included to the left of the $\chi^2/N$ values. This $P$ curve gives the probability that the $\chi^2/N$ is due to statistical fluctuations only. The expectation value for $\chi^2/N$ is 1, provided the theory fits the data and errors are entirely due to counting statistics. From a comparison of the $\chi^2/N$ values for the unshifted and shifted data, it seems clear that significantly better fits are obtained for the shifted energy scale. The results for the shifted data in Fig. 12 are therefore likely to be the most useful in a $\chi^2$ test used to decide on the need for a two-component theory. Most of the $\chi^2/N$ values in Fig. 12 range close to 1, where the probability curve is a rapidly varying function of $\chi^2/N$. At the higher temperatures, i.e., greater than about 2.5 °K, the one- and two-parameter models fit the data about equally well and both give high-probability fits based on the $\chi^2$ table. At the lowest temperature reached, i.e., 1.27 °K, the two-parameter theory gives a $\chi^2$ value corresponding to a probability of 24% while the one-parameter theory gives a fit with a probability of only 1%. At temperatures between 1.3 °K and $T_\lambda$, the two-parameter theory gives $\chi^2/N$ values which are lower than those for the one-parameter theory, but the probabilities in both cases are high, thus preventing a choice between the two models. Near $T_\lambda$, or at 2.3 °K, the $\chi^2/N$ values indicate that the two-parameter model fits better than the one-parameter model although both models give fairly low probabilities, 3 and 10% for the one- and two-parameter models, respectively. Aside from the results at $T \simeq T_\lambda$, the trend of the $\chi^2/N$ values and associated probabilities are consistent with a two-component model for neutron scattering from liquid-$^4$He atoms at $T < T_\lambda$, while above $T_\lambda$ a single-component model adequately fits the data.

The $F$ test has also been applied to all the results shown in Figs. 11 and 12. In order to obtain a summary of the predictions made by this statistical test, the joint and geometric mean probabilities were determined for four groups of results, i.e., for the shifted and unshifted data at $T > T_\lambda$ and at $T < T_\lambda$. The joint probabilities are found by multiplying all the separate probabilities together, for data in one of the groups, e.g., for unshifted data at $T > T_\lambda$. The geometric mean probability is the $n$th root of the joint probabilities, where $n$ is the number of separate experiments which were used to compute the joint probability. A total of eight experiments above $T_\lambda$ and eleven experiments below $T_\lambda$ were used to obtain the combined $F$ statistics. Table III lists the results for the combined probabilities. The geometric mean probability should be understood as giving the probability that one would obtain a value of $\chi^2$ as high or higher based on the hypothesis that the one- and two-parameter theories fit the data equally well. For example, for $T > T_\lambda$ and unshifted data, there are 123 chances out of 1000 to support this hypothesis, while for $T < T_\lambda$ there are only 13 chances out of 1000 that the two models are equivalent. For the data which have been shifted prior to least-squares fitting, the probabilities are 42 per 1000 and 5.5 per 1000 for $T > T_\lambda$ and $T < T_\lambda$, respectively. These combined probabilities do not strongly favor the choice of a two-parameter model for $T < T_\lambda$. However, they do show a trend which is consistent with the idea that at $T > T_\lambda$ a one-parameter theory adequately represents the data, while at $T < T_\lambda$ a two-parameter theory gives a better fit than a one-parameter theory. A further grouping in Table III, i.e., for $T > 2.62$ °K, indicates that for temperatures more than about 1.0 °K above $T_\lambda$ the one-parameter model provides a rather good fit to the experimental data. Six independent experiments were used to compute the combined statistic for $T > 2.62$ °K.

The values of the condensate fraction $\rho_0/\rho$ obtained from the least-squares fits of the two-parameter PT theory to the neutron scattering peaks are presented in the lower parts of Figs. 11 and 12. The value shown for unshifted data at 1.27 °K is the same as that reported in Ref. 9. Values of $\rho_0/\rho$ using the two-parameter model for $T > T_\lambda$ are listed in Table IV. While a two-parameter model is physically absurd above $T_\lambda$, this does provide some information concerning the sensitivity of the present model-experiment comparison. From the statistical evidence discussed above, it is clear that the one-parameter model fits the data as well as the

TABLE IV. Values of "false condensate" obtained by using two-parameter model to fit the helium data above $T_\lambda$.

| Unshifted data | | Data shifted 1% | |
|---|---|---|---|
| $T$(°K) | $\rho_o/\rho$(%) | $T$(°K) | $\rho_o/\rho$(%) |
| 4.20 | 2.38 ± 1.4 | 4.20 | 2.45 ± 1.1 |
| 3.83 | -1.37 ± 2.5 | 3.83 | -2.16 ± 2.3 |
| 3.16 | 2.89 ± 2.8 | 3.16 | 4.36 ± 2.2 |
| 3.00 | 5.05 ± 2.5 | 3.00 | 3.75 ± 2.2 |
| 2.62 | 5.83 ± 2.2 | 2.62 | 5.31 ± 1.8 |
| 2.30 | 4.88 ± 1.7 | 2.30 | 5.47 ± 1.5 |

two-parameter model for $T$ substantially greater than $T_\lambda$, and therefore even from a purely mathematical viewpoint $\rho_0/\rho$ can be set equal to zero for this temperature range. There does not seem to be a direct quantitative method of assessing unknown systematic errors in the model-experiment comparison. While the "false-condensate" determinations bear on this question, it is not clear how this should be factored into an over-all error estimate for the parameters. Consequently, the errors quoted on these parameters are lower limits obtained from counting statistics only. However, it should be emphasized that the $\chi^2/N$ values in Fig. 12 are in the neighborhood of 1.0, indicating that errors aside from the known statistical errors are probably small.

The condensate fractions at 1.27° are (7.5 ± 1.6)% and (8.8 ± 1.3)% for the unshifted and shifted data, respectively. Since the shifted data give better $\chi^2$ fits, it is felt that (8.8 ± 1.3)% is our best determination of $\rho_0/\rho$ from the $E_1 = 171.5$ meV data. The fractional condensate density obtained from the single $E_1 = 343$ meV experiment, at 1.28 °K, is (15.6 ± 3.7)%. This value for $\rho_0/\rho$ is larger than the (8.8 ± 1.3)% obtained from the $E_1 = 171.5$ meV experiments at $\simeq 1.27$ °K. However, these results do overlap well within twice the range of the standard errors. Since the resolution was better for $E_1 = 171.5$ meV and a series of experiments were carried out with this $E_1$ compared to only one experiment with $E_1 = 343$ meV, it is felt that the 8.8% value for $\rho_0/\rho$ is probably the more accurate one. These fractional densities are consistent with the theoretical estimates of 8–25% obtained in Refs. 1–5 for the ground-state condensate fraction. Values for average kinetic energy per liquid-helium atom are given in the central parts of Figs. 11 and 12. Results for the one- and two-parameter models are both plotted for comparison, and they overlap to within the error bars although there is a systematic difference. Error bars are shown for the two-parameter results only; errors for the one-parameter fits are comparable. The one-parameter results above $T_\lambda$ and the two-parameter results below $T_\lambda$ should provide the most accurate determination of the kinetic energy. Equation (4) has also been used to compute the $K(T)/N$ for $T > 0$ °K. In this computation, the value of $P(T=0)$ was taken as $-180$ cal/mole or $-21.65$ °K/atom,[22] and values of the latent heat were from Ref. 14. The computed $K/N$ values are shown in Figs. 11 and 12. As previously mentioned, the PE was assumed to vary with the liquid density at finite temperatures. The computed kinetic energies for the $E_1 = 171.5$ meV are approximately 1–2 °K higher than the experimental results. There is considerable uncertainty regarding the best choice for $P(T=0)$. We have found differences of at least several °K in our calculations of the PE from Eq. (5). Other workers[18] have noted the same uncertainties. The computed and measured results on Figs. 11 and 12 are therefore judged to be in agreement within the known uncertainties on the potential energy. If the experimental kinetic energies are extrapolated to absolute zero using the computed result as a guide for the temperature dependence below 1.27 °K, a $K(T=0)/N$ of about 13 °K is obtained. This is in good agreement with the recent theoretical determinations of the ground-state kinetic energy, Refs. 3, 5, and 23.

Values for $K/N$ were also obtained from the $E_1 = 343$ meV data at 1.28 and 4.20 °K. The least-squares fit of the two-parameter theory to the 1.28 °K data gives a $K/N$ of 15.1 ± 1.5 °K compared to 13.3 ± 0.5 °K from the $E_1 = 171.5$ meV data at 1.27 °K helium temperature. At a helium temperature of 4.20 °K, the one-parameter PT theory gives a value of 18.1 ± 1.7 °K for the $K/N$ compared to 15.0 ± 0.5 °K from the lower-energy $E_1 = 171.5$ meV data. Agreement between these $K/N$ values is within twice the standard errors. The higher-energy results are in better agreement with the $K/N$ calculated from Eq. (4). However, there were only two experiments carried out with $E_1 = 343$ meV compared to 19 experiments for $E_1 = 171.5$ meV. Results for the kinetic energy obtained from the latter set of experiments are therefore judged to be more accurate.

## V. SUMMARY AND DISCUSSIONS

High-energy and momentum-transfer neutron scattering was used to obtain information about the motions of liquid-$^4$He atoms. Scattering experiments were performed with much higher energy and momentum transfers than were used in previous studies of liquid helium. Momentum wave-vector transfers up to 20.3 Å$^{-1}$ were reached along the free-particle excitation curve. A primary objective of this research was to test the suggestion that at sufficiently high momentum transfers, where neutrons are expected to scatter from single helium atoms, structure might be observable in the cross-section peaks which could be identified with the Bose-Einstein or zero-momentum condensate.

At the higher values of momentum transfer the measured recoil energies, as well as the behavior of the single-differential cross sections, is consistent with a single-particle model for the scattering. Above the $\lambda$ temperature the scattering peaks are found to be well represented by the free-particle scattering function, i.e., a single Gaussian in $\hbar\omega$ at constant $\kappa$. Below $T_\lambda$ there appears to be additional structure in the scattering peaks and a single-component free-particle model does not fit as well as it does for $T > T_\lambda$. A marked change in the temperature dependence of the scattering peak widths occurs near the $\lambda$ point. The observed behavior is

consistent with a transition in which a second narrow component, such as might be caused by a momentum condensate, begins to contribute to the scattering cross section.

A theory[19] with only two variable parameters, the kinetic energy per helium atom and the fractional condensate density, along with a free-particle form for the scattering function, has been used to interpret the measured cross sections. Statistical analysis of the least-squares fits of this theory to the experiments indicates that the two-component model, which includes a condensate fraction, gives a good fit to scattering cross sections for $T < T_\lambda$, while above $T_\lambda$ a one-component model, with a zero-condensate fraction, will give a good fit to the data. Values of the kinetic energy per atom and the condensate fraction are obtained from the theory-experiment comparison for temperatures in the range 1.27–4.20 °K. The condensate fractions obtained in this way range $(7.5 \pm 1.6)$–$(8.8 \pm 1.3)$% at 1.27 °K depending upon the method of analysis used, the 8.8% value is judged to be the most accurate. Errors quoted for the parameters represent the effects of statistical counting errors in the least-squares-fitting analysis. No assessment of unknown systematic errors seemed feasible although the discussion attempts to provide an objective picture of possible uncertainties in the model-experiment comparison. These results are consistent with recent theoretical estimates for the ground state of liquid helium. Values for the kinetic energy per atom have also been deduced from the theory-experiment comparison. The neutron scattering results for kinetic energy are compared to the kinetic energy computed from thermodynamic phase equilibria considerations. The shape of the temperature dependence as well as the magnitudes of the kinetic energies, obtained from the present experiments, are in agreement to within known uncertainties with the computed results.

Additional measurements of the type reported here would be desirable at lower and higher liquid-helium temperatures than the range covered in the present study. Further measurements at substantially lower temperatures are judged to be particularly important since they could provide the necessary leverage to give a more definitive answer to the question of momentum condensation. Measurements at significantly lower temperature, for example, down to ~0.5 °K, would also provide kinetic-energy results in a range where this quantity is expected to be quite flat. This would permit accurate extrapolation to absolute zero where a direct comparison can be made with various theoretical results.

## ACKNOWLEDGMENTS

The author would like to acknowledge substantial help from Dr. W. D. McCormick during the preparatory phase of the measurements presented here. Several useful discussions were held with Dr. R. D. Puff during the course of the research. The author is also particularly indebted to Dr. J. G. Couch for numerous contributions during his stays at Hanford as a summer faculty appointee under the USAEC NORCUS program. Mrs. P. Z. Aldridge and K. B. Stewart provided competent help in data processing. B. H. Duane provided expert help in the programming for and use of program LIKELY. R. L. Hooper and Dr. D. A. Kottwitz provided advice for the statistical interpretation. Dr. C. W. Lindenmeier and Dr. L. C. Schmid have supported this work in a number of ways.

---

†Work performed under the U.S. Atomic Energy Commission Contract No. AT(45-1)-1830 and supported in part by the Battelle Memorial Institute.

[1]O. Penrose and L. Onsager, Phys. Rev. 104, 576 (1956).

[2]F. London, *Superfluids* (Wiley, New York, 1954), Vols. I and II.

[3]W. L. McMillan, Phys. Rev. 138, A442 (1965).

[4]W. E. Parry and C. R. Rathbone, Proc. Phys. Soc. (London) 91, 273 (1967).

[5]Daniel Schiff and Loup Verlet, Phys. Rev. 160, 208 (1967).

[6]P. C. Hohenberg and P. M. Platzman, Phys. Rev. 152, 198 (1966).

[7]R. W. Cowley and A. D. B. Woods, Phys. Rev. Letters 21, 787 (1968).

[8]A. D. B. Woods and R. W. Cowley, in *Proceedings of the Fourth Symposium on Neutron Inelastic Scattering, Copenhagen, Denmark* (IAEA, Vienna, 1968), Vol. I, p. 609.

[9]A brief report of this work has been published by O. K. Harling, Phys. Rev. Letters 24, 1046 (1970).

[10]O. K. Harling, Rev. Sci. Instr. 37, 697 (1966); in Ref. 8, Vol. II, p. 271.

[11]This normalization was accomplished by setting the sum over angle and energy of the differential cross sections equal to $\sigma_t$, the expected total cross section. The value of $\sigma_t$ was taken from I. Langner, J. J. Schmidt, and D. Woll, Kern Forschungs Zentrum Karlsruhe, Report No. 750, 1968 (unpublished).

[12]V. F. Sears, Phys. Rev. 185, 200 (1969).

[13]Equation (1) is strictly correct only for scattering off stationary atoms; however, it can be shown [A. G. Gibbs (private communication)] that the finite-temperature gas-scattering result also reduced to Eq. (1) when the initial neutron energy is much larger than the kinetic energy of the gas atoms.

[14]W. B. Keller, *Helium-3 and Helium-4* (Plenum, New York, 1969), p. 112.

[15]Alan G. Gibbs and O. K. Harling, Phys. Rev. A (to be published).

[16]D. G. Henshaw, Phys. Rev. 119, 9 (1960).

[17]E. K. Achter and L. Meyer, Phys. Rev. 188, 291 (1969).

[18]L. Goldstein and J. Reekie, Phys. Rev. 98, 857 (1955).

[19]R. D. Puff and J. S. Tenn, Phys. Rev. A 1, 125 (1970).

[20]B. H. Duane (BNW Program LIKELY), U.S. AEC formal document No. BNWL-390, 1967 (unpublished).

[21]$\chi^2$ is defined as the sum of the squares of the differences between theory and experiment weighted by the inverse of the squares of the experimental errors, these errors are derived from counting statistics only. $N$ is the number of independent data points being fitted, reduced by the number of fitting parameters.

[22]K. R. Atkins, *Liquid Helium* (Cambridge U. P., Cambridge, England, 1959).

[23]W. E. Massey and C. W. Woo, Phys. Rev. 164, 256 (1967).

PHYSICAL REVIEW A VOLUME 3, NUMBER 3 MARCH 1971

# Experimental Observation of the Drift Dissipative Instability in an Afterglow Plasma

M. W. Alcock and B. E. Keen
*United Kingdom Atomic Energy Authority Research Group, Culham Laboratory, Abingdon, Berkshire, England*
(Received 1 May 1970)

Measurements are reported on low-frequency self-excited oscillations in an inhomogeneous afterglow plasma, in which there is a radial density gradient perpendicular to an axial homogeneous magnetic field. The plasma was produced either by using a short pulse of electrons emitted from a hot cathode to ionize the background gas, or by pulsing off an rf discharge. The plasma so formed had an initial density of $\sim 10^{10}$ ion cm$^{-3}$ and a temperature $T_e \sim 1000$ °K. The experiment was carried out using tubes of 2.5 and 5.0 cm diam, giving inverse density scale lengths for the radial density gradient of $\sim 2.3$ and $\sim 1.3$ cm$^{-1}$, respectively. The oscillations occurred mainly as $m = +1$ azimuthal modes although some results for $m = +2$ were obtained. The oscillations were shown to be standing waves in the axial direction $z$ with a wavelength $\lambda_z$, approximately equal to the column length. It was found that the frequency of oscillation $\omega$ was dependent on the column length and by varying this, a dispersion relationship $\omega$ vs $k_z = (2\pi/\lambda_z)$ could be plotted under various conditions. It was found that the frequency was independent of time (or density) in the afterglow and that the frequency of oscillation tended to zero as $k_z \to 0$ and to $\omega^*$ as $k_z$ assumed larger values. The simple theory of drift dissipative instabilities has been extended to include effects due to electron-neutral and ion-neutral collisions and the Re($\omega$), and growth rates Im($\omega$), vs $k_z$ have been calculated for the relevant experimental cases. Comparison of theory and experiment shows remarkably good agreement considering the possible errors in some of the experimental quantities and the assumptions present in the theory.

## I. INTRODUCTION

During the last few years there has been much interest in the low-frequency oscillations or instabilities occurring in inhomogeneous magnetoplasmas. This is due to the possible anomalous cross-field diffusion caused by the presence of these microinstabilities. Of particular interest are those instabilities occurring in a plasma with a density gradient perpendicular to the containing magnetic field in the cases where collisions between particles or lack of collisions may lead to oscillations. These self-sustained oscillations are the so-called drift instabilities, and their main properties in both the collisional and collisionless regimes have been summarized by Kadomtsev[1] and Mikhailovski.[2] Unfortunately, in most experiments on drift waves reported to date, large radial electric fields as well as radial density gradients have existed in the plasma. This electric field, together with the longitudinal magnetic field, leads to an azimuthal rotation of the plasma, and consequently causes a Doppler shift in the instability frequency, usually of the same order of magnitude as the drift frequency itself.[3-6] Further, it has been shown[7] that in an inhomogeneous plasma a rotationally convected drift-wave type of instability can be supported if collisions exist in the presence of this radial electric field.

In afterglow plasmas, however, this radial electric field is small (experimentally found to be of the order of 10 mV/cm), and most of the other possible causes of instability such as axial current, nonisotropic velocity distributions, and imposed electric fields are absent. Therefore, most experiments on afterglow plasmas had shown them to be stable, but recently Pigache and Harding[8] have reported the observation of drift waves in a helium afterglow. This paper reports further results obtained in both helium and hydrogen afterglow plasmas on a low-frequency instability. Experiments have been performed in two different tubes, thus varying the density gradient scale length, and in different axial magnetic fields. The instability